Lasers in Manufacturing Conference 2023

Process-structure-property relationships of additively manufactured lattice structures based on triply periodic minimal surfaces (TPMS)

F. Günther[a,b,*], M. Wagner[b], S. Pilz[c], A. Gebert[c], M. Zimmermann[a,b]

[a]*TU Dresden, Helmholtzstraße 7, 01069 Dresden, Germany*
[b]*Fraunhofer IWS, Winterbergstraße 28, 01277 Dresden, Germany*
[c] *Leibniz IFW Dresden, Helmholtzstraße 20, 01069 Dresden, Germany*

Abstract

Lattices based on triply periodic minimal surfaces (TPMS) are attracting increasing interest due to their excellent structure-property relationships. However, the potential can only be exploited if their structural integrity is ensured. This requires a fundamental understanding of the impact of imperfections that arise during additive manufacturing. Therefore, in the present study, the structure-property relationships of TPMS lattices, including their imperfect morphologies, are investigated experimentally and numerically. Specifically, the focus is on biomimetic TPMS lattices fabricated by laser powder bed fusion (LPBF) from the biocompatible alloy Ti-42Nb. Based on computed tomography analyses, typical LPBF-imperfections are identified before a modeling procedure is developed for reconstruction of the as-built morphology. Finally, compression tests are performed and compared with the accompanying finite element studies. This work highlights the central importance of process-related imperfections for the structure-property relationships of LPBF-processed TPMS lattices and provides a numerical tool to capture their effects. Given high simulation accuracy and flexibility, this approach might become a key factor in the future design process of additively manufactured structures.

Keywords: lattice structures; triply periodic minimal surfaces; additive manufacturing; imperfect lattices; numerical reconstruction

1. Introduction

Lattice structures based on triply periodic minimal surfaces (TPMS) have emerged as an attractive option for various industrial applications. This is especially true for bone tissue engineering (BTE), in which implants are developed to replace injured bone. The keen interest in TPMS lattices is explained by the variety of

exceptional properties, which helps to reduce the risk of the stress-shielding effect while maintaining the required minimum strength [Günther et al., 2022a]. Due to its biocompatibility and low Young's modulus, permanent implants are mostly made of titanium and its alloys. Recent work has focused on the development of beta-Ti alloys, such as Ti-42Nb [Pilz et al., 2022], and their additive manufacturing (AM). Given the high design flexibility, laser powder bed fusion (LPBF) is the most widely used technology [Benedetti et al., 2021].

TPMS based scaffolds have already been extensively fabricated and tested. Besides the convincing structure-property relationships [Kelly et al. 2021], however, the impact of process-related imperfections became apparent. Here, imperfection refers to any target-actual deviation occurring during production. Usually, internal and external imperfection are distinguished: the first class concerns imperfections in the microstructure such as pores, whereas the second class includes all surface phenomena such as roughness and shape deviation [Echeta et al., 2020]. Internal imperfections can be significantly reduced by process parameter optimization or post-treatment. In contrast, external imperfections of 50-500 µm in size remain a major issue of LPBF processed structures: although surface roughness can be partially eliminated, the larger shape deviations can only be insufficiently avoided [Al-Ketan et al, 2019].

Since imperfections have a critical impact on the performance of lattices, research aims at a deeper understanding of process-structure-property relationships. Here, finite element (FE) analysis plays an increasingly important role, where modeling routines artificially reproduce the essential features of the as-built morphology [Lozanovski et al., 2019]. For TPMS lattices, the foundation in this branch of research was laid with our previous work [Günther et al., 2022b], but the effectiveness has only been demonstrated on a single lattice so far. This is where the present study comes in: by validating against a comprehensive experimental matrix, the numerical tool of reconstruction shall be unlocked for a wide range of users.

2. Methods

Detailed information on the methods of modeling, material, fabrication, and testing are provided in our previous work [Günther et al., 2022a; Günther et al., 2022b; Pilz et al., 2022]. The specimens are based on the TPMS types Schoen I-WP and Gyroid in network configuration and have a volume fraction of 25%. The lattices are obtained by the relation $\phi + r = 0$, where ϕ denotes the level set equation of a TPMS and r the level set constant controlling the volume fraction. To investigate the influence of TPMS type and cell size, four variants are considered. They are specified in Tab. 1 and Fig. 1.

Tab. 1: Considered TPMS network lattices with 2x2x2 unit cells and 25% volume fraction.

notation	TPMS	cell size / mm
I-2	I-WP	2
I-4	I-WP	4
G-2	Gyroid	2
G-4	Gyroid	4

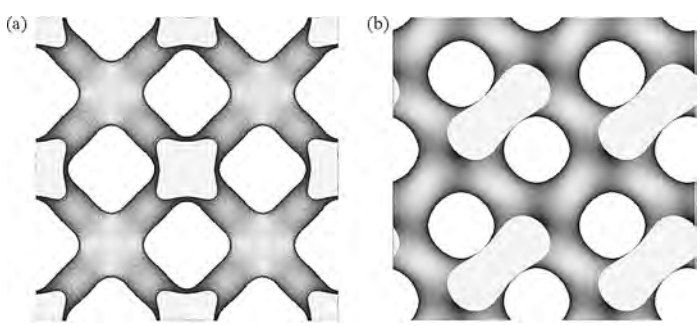

Fig. 1. Idealized as-designed configuration of the (a) I-WP and (b) Gyroid lattice.

The specimens are fabricated from a Ti-42Nb alloy by LPBF. A SLM 280 Generation 2.0 dual-laser machine (SLM Solutions Group AG, Germany) equipped with an infrared laser source with a Gaussian beam profile and 80 µm beam size is used. Here, a laser power of 210 W, a scan speed of 1050 mm/s, a hatch distance of

100 µm, a layer thickness of 50 µm and a scan rotation of 67° are applied. The lattices are removed from the build plate by spark erosion and ground plane-parallel.

µ-CT measurements, including 360° scans, are performed using a GE Phoenix Nanotom M (Waygate Technologies, Germany) on one specimen per variants. Thus, the manufacturing quality is monitored, and the material density and the volume fraction are measured (VGSTUDIO max 2022.2, Volume Graphics, Germany). The voxel size resolution is 5.2 µm. For volume reconstruction, the software Phoenix datos|x 2.2 (Baker Hughes, USA) is used. For mechanical characterization, uniaxial quasi-static compression tests are performed with a tension-compression module (Kammrath & Weiss GmbH, Germany) with a 10 kN load cell and a strain rate of 0.125 min^{-1}. To study the influence of the loading direction with respect to the build direction (BD), tests are conducted parallel and perpendicular to the BD. During the tests, the force in the load cell and the crosshead travel of the testing machine are measured. Nominal strains are calculated by relating the displacement to the initial lattice height and nominal stresses by relating the force to the initial cross-sectional area. The effective compressive stiffness $\overline{E}$ and the effective compressive yield strength $\overline{\sigma}_y$ are each determined from the average of three individual results. Note that the stiffness is determined as the slope of the regression line in the range of 5-15 MPa. In addition, the experiments are measured with a microDAC video extensometer and the in-plane von Mises strain σ_v is evaluated by digital image correlation (DIC) using VEDDAC 7 software (Chemnitzer Werkstoffmechanik GmbH, Germany).

In order to reconstruct the imperfect morphology of additively manufactured structures, a previously developed modeling procedure [Günther et al., 2022b] is adopted. The modeling is done using MATLAB (USA) software, where the *z*-direction corresponds to the BD. For distinction, the ideal CAD lattice is called as-designed model, the lattice derived directly from CT data is called as-built model, and the artificially modeled lattice is called reconstructed model. In the reconstruction procedure, the material of the as-designed model is redistributed in three steps. Firstly, the excess material is modeled on the overhanging surfaces. For a slope-dependent amount of excess material, the Zenith angle θ between the slope of the lattice surface and the *z*-axis is determined. Then, the *z*-coordinate of all surface nodes is shifted by the sigmoid function

$$g_1(\theta) \coloneqq C_3 + \frac{C_4 - C_3}{1 + \exp[C_1(C_2 - \theta)]}, \tag{1}$$

where C_1 to C_4 control the course of the function. In the second step, the surface roughness is generated by repeatedly shifting the surface nodes slightly with random size and direction. Specifically, an iteration loop is executed defining a random point within the design domain of the lattice and a random direction. Based on these quantities, the surface is shifted depending on the position. During one iteration, the direction of the shift remains constant, whereas the magnitude depends on the distance d to the random point according to

$$g_2(d) \coloneqq C_5 \exp(-C_6 d)\,. \tag{2}$$

Again, C_5 and C_6 are modeling constants to be specified. The surface shifting is looped 2000 iterations per unit cell. To match the volume fraction φ of the reconstructed model to that of the as-built model after material redistribution, the level set constant *r* is readjusted in the third step.

The modeling constants C_1 to C_6 are calibrated to minimize the relative Boolean difference volume Δ_{BOOL} between the as-built and the reconstructed model. Δ_{BOOL} is calculated by first subtracting the bounding volume of the reconstructed model from that of the as-built model, and then by dividing the remaining volume by the design space volume. This measurement is done with nTopology (USA) software. Unlike the volume fraction φ, which is the same in all three models, the relative Boolean difference volume Δ_{BOOL} indicates the morphological similarity and is therefore used. To facilitate the comparability of the different variants, a cell size related representation is used for the shifts g_1 andg_2. Furthermore, besides the level set constant *r* only

their respective scaling parameters C_4 and C_5 are varied. Note that no unique lattice design is obtained due to the semi-stochastic procedure. Therefore, three lattices are considered for each parameter set and the standard deviation is given. An overview of the modeling procedure is given in Fig. 2.

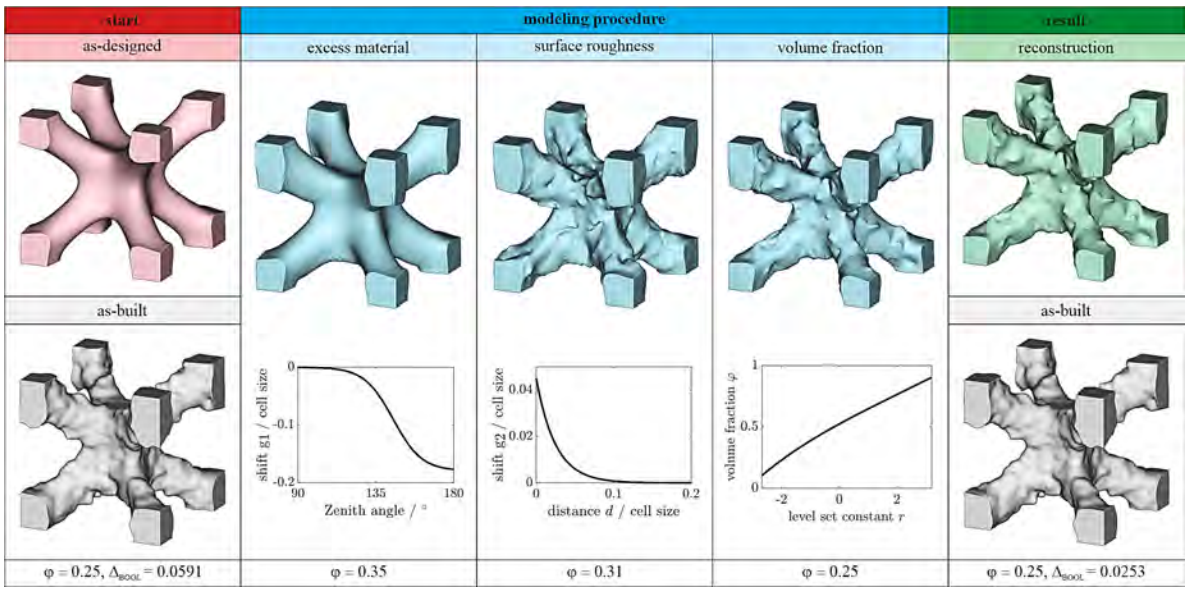

Fig. 2. Illustration of the TPMS lattice reconstruction. Detailed information is provided in our previous work [Günther et al., 2022b].

The structural mechanical FE simulations are performed with Pam-Crash 17.5 software (ESI Group, France) using the explicit solver. The triangular surface meshes are converted into tetrahedral FE volume meshes with quadratic shape functions using nTopology software. To capture the tensile and compressive material behavior of LPBF-processed Ti-42Nb, the FE material model includes orthotropic elasticity and Raghava-Hill plasticity. Note that failure is not modeled, as the focus of this study is on predisruptive behavior. For the boundary conditions, two rigid plates are modeled at the top and bottom of a lattice. A surface-to-surface contact condition is used between the plate and lattice with a friction coefficient of 0.3. Self-penetration of the lattice is excluded by an additional contact condition. All degrees of freedom of the lower plate are restricted, whereas the upper plate is displaceable only in *z*-direction. The displacement applied to the upper plate is $\overline{u} = \overline{\varepsilon} l$ with the effective nominal strain $\overline{\varepsilon} = -0.3$. During compression, the reaction force and displacement are captured. From this history variables, nominal stress-strain curves are calculated. Furthermore, the nominal compressive stiffness $\overline{E}$ and the nominal compressive yield strength $\overline{\sigma}_{\mathrm{y}}$ are considered for the mechanical characterization. Finally, the contour plot of the von Mises equivalent strain $\overline{\varepsilon}_{\mathrm{v}}$ is analyzed.

3. Results

The results of the target-actual comparison between as-designed and as-built state from the CT scans are compiled in Fig. 3. Although the TPMS morphology is principally well represented, two types of imperfections are observed: firstly, partially melted powder particles adhere evenly distributed over the entire surface, resulting in increased roughness. From the spatial deviation plots in Fig. 3(a), the associated deviation is between ±100 µm. For implants, a surface roughness of up to 8.5 µm is positive for osseointegration [Ataee et al., 2018]. From a mechanical perspective, however, roughness is an issue that likely needs to be addressed,

as the notch effect affects load-bearing capacity. The second type of imperfection concerns the excess material on overhanging surfaces. This becomes noticeable from an overhang of 45° and increases with increasing angle up to 400 µm. From the auxiliary circles drawn with the ideal pore size, it is apparent that excess material depends on the cell size: here, the smaller the cell size is, the greater is the relative amount. In terms of process physics, the phenomenon is attributable to local overmelting because of impeded heat conduction. Consequently, the amount of excess material can be reduced by selectively reducing the energy input at the overhanging surfaces [Benedetti et al., 2021]. Moreover, excess material is differently located in the lattices: while excess material in the I-WP lattice occurs mainly at the bottom of the nodes, in the Gyroid lattice it is also present below the struts. Ultimately, excess material entails a directionality of as-built morphology, whose mechanical implications will be explored later.

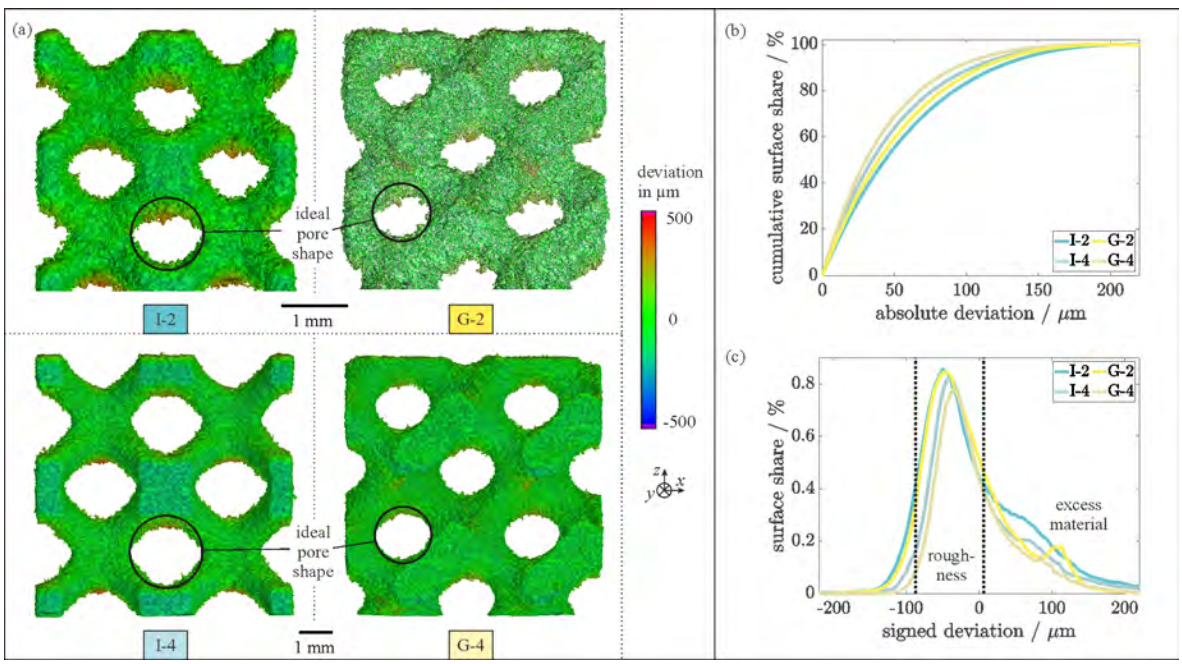

Fig. 3. Morphological data from µ-CT scans: in (a), the three-dimensional deviation plots are shown, and in (b) and (c), the distributions absolute and signed deviation. The quantities refer to the deviation between the as-designed and the respective as-built model.

Using the absolute deviation plot in Fig. 3(b), the size effect of imperfections can be further specified: accordingly, not only the relative deviation decreases with increasing cell size, but also the absolute deviation. This finding is explained by the improved heat dissipation due to the larger material volume, resulting in less partially melted particles. Upon further investigation, the 90% deviation quantiles were found to be between 93-121 µm, with greater deviation for I-WP lattices than for the Gyroid counterparts. This finding confirms conjectures from previous work [Günther et al., 2022b] evaluating the LPBF-related criticality of TPMS lattices. In particular, about 15% of surface of the I-WP has an overhang of at least 45°, compared to 11% for the Gyroid lattice. Furthermore, the volume fraction is shown to exceed the target value of 25% for all models, with values ranging from 26.2% to 27.3%. In general, exceeding the target volume fraction is a commonly observed phenomenon in PBF-processed components, which is due to the extrusion-like nature of the excess material [Echeta et al., 2020]. This is illustrated by the positive skewness of the signed deviation graphs in Fig. 3(c). Finally, microporosity measurements yield values of less than 0.2%, indicating good LPBF process control.

Based on the evaluation of the as-built morphology, the reconstruction is performed. Fig. 4 contains the side views of all as-designed, as-built and reconstructed models, as well as their morphological metrics in terms of relative Boolean difference volume Δ_{BOOL} and mean absolute deviation MD. Overall, the effectiveness of the modeling procedure is demonstrated as the morphological similarity between the reconstructed and as-built models is significantly higher than that between the as-designed and as-built models: in particular, Δ_{BOOL} decreases approximately by half, and MD largely matches that of the CT measurement. However, there is still a discrepancy between the as-built and the reconstructed models: on the one hand, this can be attributed to the fact that three reconstructions are used for each variant. This avoids overfitting the modeling parameters, but the reconstruction is not optimal for a single specimen. On the other hand, the reconstruction procedure does not reflect the particular defect susceptibility of peripheral lattice zones. Consequently, although the modeled degree of imperfections is similar on average to the as-built lattice, it is too small at the lattice periphery and too large at the center. Comparing the morphological metrics Δ_{BOOL} and MD, two important observations emerge: firstly, both metrics tend to correlate. Thus, the regularities found for the absolute deviation in principle also apply to the relative Boolean difference volume. However, this tendency is overlaid by a second effect: Δ_{BOOL} decreases by up to 93% when the cell size is doubled, while MD only decreases up to 16.3%. This difference is due to the geometrical size effect, which is only reflected in the relative Boolean difference volume but not in the mean absolute deviation. Thus, Δ_{BOOL} proves to be a more pertinent descriptor for the effective morphological similarity of two structures than MD.

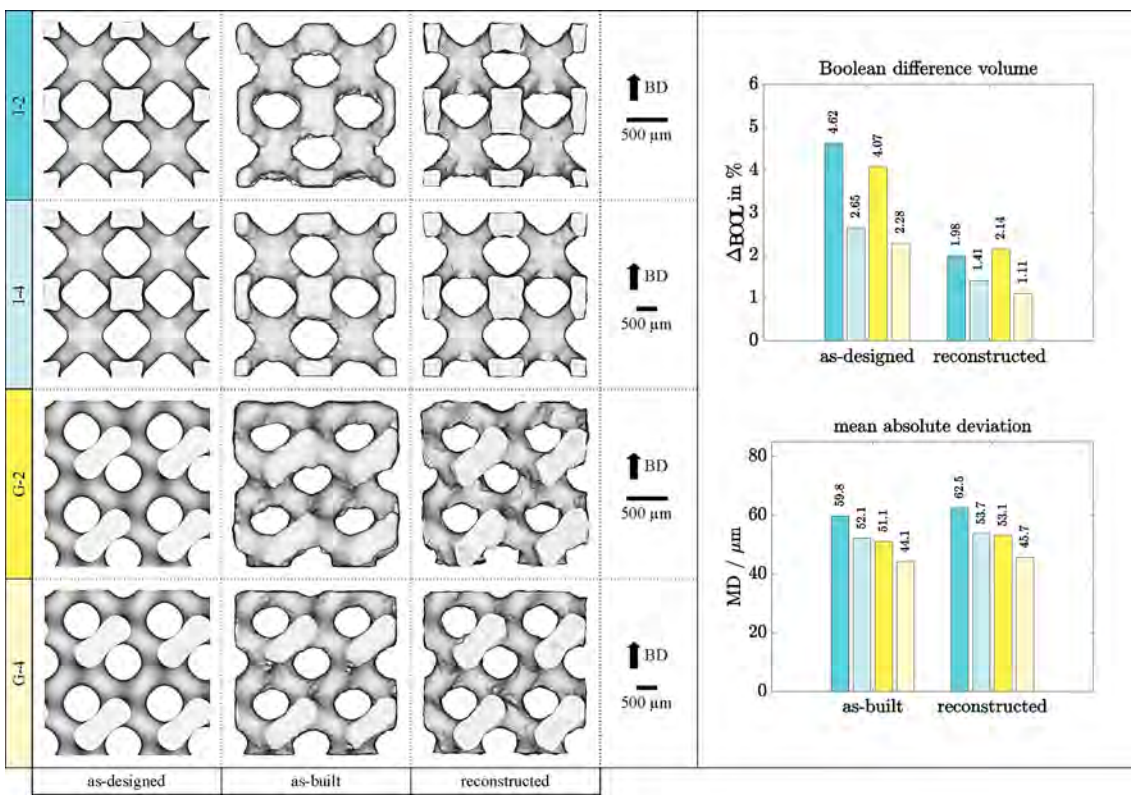

Fig. 4. Morphological results: Δ_{BOOL} is the relative Boolean difference volume to the as-built model and MD is the mean absolute deviation to the as-designed model.

The nominal stress-strain curves of the uniaxial compression tests are shown in Fig. 5(a). In general, a pronounced plastic domain with horizontal curve progression is observed for all variants and test directions. In particular, the lattices pass 30% nominal strain without abrupt failure, which contributes to a safe implant application in BTE. In addition, the nominal compressive stiffnesses less than 1 GPa, are suitable for the development of stiffness-neutral implants. However, as with the morphology, cell size is reflected in the mechanical results: for both TPMS types, the 4 mm unit cell size is associated with improved mechanical performance in terms of stiffness and strength compared to the reference variants. This is due to the better process fidelity or the lower degree of imperfections, cf. Fig. 4. Moreover, stiffness and strength are found to decrease for parallel test direction (||) compared to perpendicular direction (⊥). This directionality of mechanical properties can be attributed to the excess material causing morphological anisotropy. However, the influence of test direction is less than that of cell size. To further investigate the compressive behavior, the in-plane von Mises strain maps in Fig. 5(b) are considered. These refer to the parallel test direction and $\overline{\varepsilon} = -0.15$ applied nominal strain. Compared to the 4 mm cell size, the 2 mm variants exhibit a more heterogeneous strain distribution. This is due to the greater influence of imperfections at smaller cell sizes. In fact, imperfections under loading cause local stress or strain concentrations that act as mechanical weak points. Furthermore, both TPMS type are characterized by different failure modes: while a layer-by-layer collapse is observed for the I-WP lattices, the Gyroid lattices fail by shear sliding 45° to the loading direction.

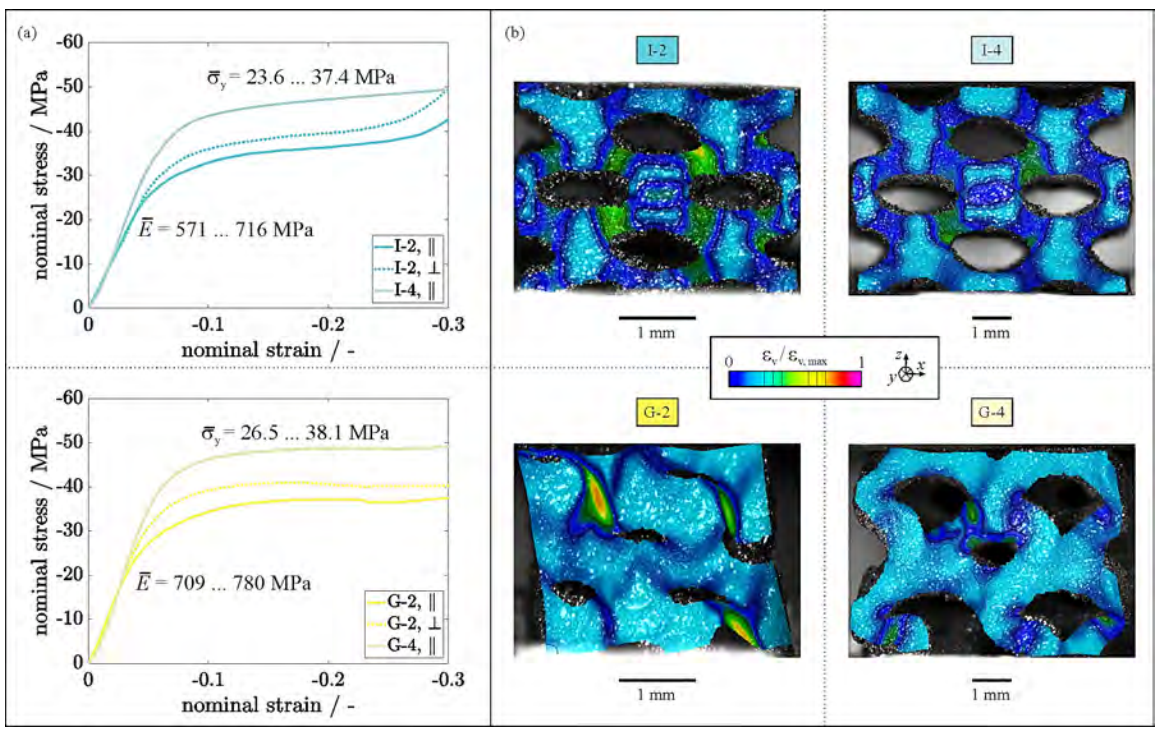

Fig. 5. Experimental results of compression tests: in (a), the averaged nominal stress-strain curves are shown for parallel (||) and perpendicular (⊥) test directions, and in (b), the in-plane von Mises strain for $\overline{\varepsilon} = -0.15$ applied nominal strain determined with DIC.

The results of numerical compression tests for parallel test direction are shown in Fig. 6. Comparison of the nominal stress-strain curves of the as-designed, as-built and reconstructed models with those of the experiment highlights two main aspects: firstly, regardless of the variant, the as-designed model overestimates

the experimentally measured compression behavior. In contrast, secondly, both the as-built and the reconstructed model accurately represent the actual behavior. Both observation are consistent with pertinent literature [Günther et al., 2022b; Lozanovski et al., 2019]. It is important to remark that the volume fraction of all models is respectively equal to that of the experiment. Thus, a direct correlation between the target-actual deviation of the as-built morphology and the mechanical degradation is observed. More precisely, the imperfections included in the reconstruction, namely surface roughness and excess material, emerge as formative factors for quasi-static mechanical performance. In contrast, microporosity and material heterogeneity appear to be less important, as the as-built and reconstructed models accurately represent the experiment even without their consideration. Causes for this finding arise from the von Mises strain distribution of the reconstructed models at a nominal strain of $\overline{\varepsilon} = -0.15$. On the one hand, excess material on overhanging surfaces is found to have subordinate load-bearing function. These ineffective material reservoirs are particularly evident in the I-WP lattices, where the excess material is located at the node bottoms. Since the total material content is constant, other structural features such as the struts are thinned, i.e., mechanically weakened. On the other hand, similar to the DIC plots in Fig. 5(b), a heterogeneous strain distribution with local peaks is shown. This is particularly pronounced in Gyroid lattices and can be attributed to the roughness-induced morphological irregularity.

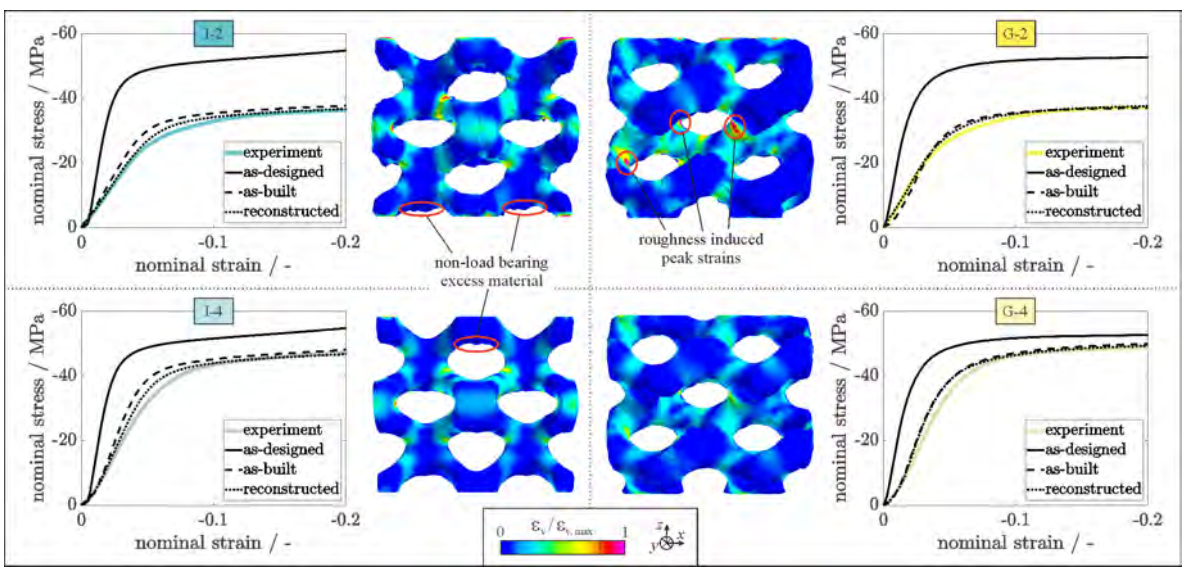

Fig. 6. Numerical results of uniaxial compression tests in parallel with BD: the nominal stress-strain curves obtained from FE simulations are compared with the experimental results, and the von Mises strain plots refer to the reconstructed lattices at $\overline{\varepsilon} = -0.15$.

The relative deviations from the experimentally measured compressive stiffness $\overline{E}$ and yield strength $\overline{\sigma}_y$ are shown in Fig. 7. As expected, the as-designed models are subject to the largest deviations. This overestimation of stiffness is up to 341% and that of yield strength up to 66%. In contrast, the as-built and reconstructed models are associated with substantially lower deviations. In comparison, the reconstructed models tend to be the most precise, with a maximum deviation of 26% for stiffness and 12% for strength. Here, it is important to note that the deviation between as-built and reconstructed does not significantly affect the nominal mechanical properties of a lattice. Therefore, the globally averaged degree of imperfection is sufficient to accurately represent the quasi-static pressure behavior, even if local variation exists. Literature review indicates the effectiveness of the presented approach: *Lozanovski et al.* [Lozanovski et al., 2019] found 23%

and 31% numerical deviation for stiffness and strength for face-centered cubic lattices, and *Radlof et al.* [Radlof et al., 2021] reported 153% and 28% for uniform cubic lattices, respectively. Since three specimens are considered for each of the experiments and reconstructed models, overfitting for a single specimen is ruled out. Furthermore, principally similar results are observed for the perpendicular test direction. Thus, the results are statistically significant, reproducible and generally valid.

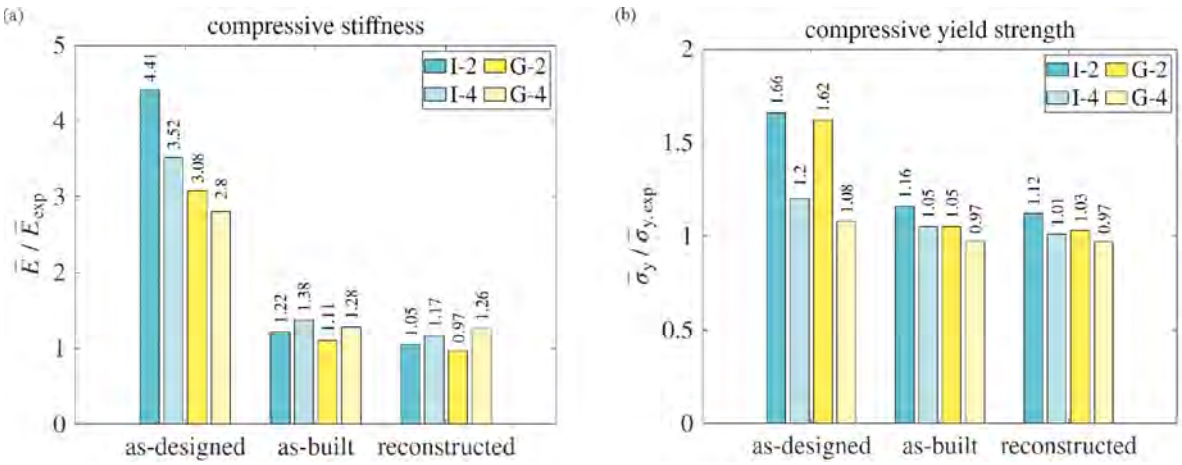

Fig. 7. Numerical compressive (a) stiffness and (b) yield strength related to the respective experimental ones for all models.

Overall, the reconstruction procedure proves to be a valuable tool for non-destructive structure-property studies. In addition to the high morphological similarity, the FE analyses on the reconstructed models attest to high simulation accuracy. This finding confirms that of previous work on a single lattice [Günther et al., 2022b]. However, by considering different TPMS types, cell sizes and loading directions, the reproducibility and generalizability of the modeling approach is now also demonstrated. In the context of BTE, high numerical accuracy can help to reduce the necessary testing effort without compromising optimal and safe application.

4. Conclusion

The process-structure-property relationships of four promising bone substitutes based on triply periodic minimal surfaces (TPMS) made of laser powder bed fused (LPBF) Ti-42Nb were investigated. The imperfect lattice morphology was examined with µ-CT scans before uniaxial compression tests were performed. Numerical work focused on reconstructing the as-built morphology, including process-related features such as roughness and excess material on overhanging surfaces. The following conclusions can be drawn:

- In the as-built state, LPBF processed TPMS lattices feature external imperfections, the extent of which depends sensitively on the lattice type and cell size. Due to the larger surface fraction with overhang exceeding 45°, I-WP lattices tend to larger target-actual deviations than the Gyroid ones. In addition, due to the lower heat capacity, the deviations are larger for 2 mm cell size than for 4 mm.
- The presented modeling procedure enables the reconstruction of the imperfect as-built morphology of TPMS lattices. Here, the relative Boolean difference volume Δ_{BOOL} with respect to the CT data proves to be a suitable descriptor of the reconstruction quality. Specifically, the reconstructed models exhibit a halved relative Boolean difference volume Δ_{BOOL} compared to the idealized as-design models.

- In uniaxial compression tests, I-WP and Gyroid lattices show excellent suitability for implant applications given high ductility, low stiffness to below 1 GPa and high yield strength to above 35 MPa. However, imperfections prove to be a formative factor for the stiffness and strength. Here, the larger the relative target-actual deviation is, the more the structural integrity is impaired. In addition, the values for the tests performed parallel to the build direction are lower than those conducted perpendicular.
- Performing finite element simulations reveals that the experimentally measured compressive behavior is drastically overestimated by the as-designed models. In particular, the overestimation of stiffness is up to 341% and that of yield strength is up to 66%. In contrast, the deviations for the reconstructed models are much smaller, with a maximum deviation of 26% for stiffness and 12% for strength.

The results encourage to use the presented methodology for further structure-property investigations. In particular, the reconstruction procedure is modified by introducing directional excess material and surface roughness. This is intended to more accurately represent the actual as-built morphology. In addition, the transferability of the modeling parameters to other TPMS lattices is investigated in order to predict structure-property relationships non-destructively and without CT measurements. Finally, other structure-property relationships such as fatigue strength and permeability of imperfect lattices are explored. If these studies confirm the general procedure, a data-driven design tool is available that greatly advances the use of laser powder bed fusion fabricated TPMS lattices for both research and industry.

Acknowledgements

The authors would like to thank the Deutsche Forschungsgemeinschaft (DFG) for funding under projects ZI 1006/16-2 and GE/1106/12-2 (No. 419952351). In addition, P. Lepper is thanked for his experimental help.

References

Günther, F., Wagner, M., Pilz, S., Gebert, A., Zimmermann, M., 2022a. Design procedure for triply periodic minimal surface based biomimetic scaffolds. Journal of the mechanical behavior of biomedical materials 126, p. 104871.

Pilz, S., Gustmann, T., Günther, F., Zimmermann, M., Kühn, U., Gebert, A., 2022. Controlling the Young's modulus of a ß-type Ti-Nb alloy via strong texturing by LPBF. Materials & Design 216, p. 110516.

Benedetti, M., Du Plessis, A., Ritchie, R., Dallago, M., Razavi, S., Berto, F, 2021. Architected cellular materials: A review on their mechanical properties towards fatigue-tolerant design and fabrication. Materials Science & Engineering R 144, p. 100606.

Kelly, C., Wang, T., Crowley, J., Wills, D., Pelletier, M., Westrick, E., Adams, S., Gall, K., Walsh, W., 2021. High-strength, porous additively manufactured implants with optimized mechanical. Biomaterials 279, p. 121206.

Echeta, I., Feng, X., Dutton, B., Leach, R., Piano, S., 2020. Review of defects in lattice structures manufactured by powder bed fusion. The International Journal of Advanced Manufacturing Technology 106, p. 2649.

Al-Ketan, O., Abu Al-Rub, R., 2019. Multifunctional Mechanical Metamaterials Based on Triply Periodic Minimal Surface Lattices. Advanced Engineering Materials 21, p. 1900524.

Lozanovski, B., Leary, M., Tran, P., Shidid, D., Qian, M., Choong, P., Brandt, M., 2019. Computational modelling of strut defects in SLM manufactured lattice structures. Materials & Design 171, p. 107671.

Günther, F., Hirsch, F., Pilz, S., Wagner, M., Gebert, A., Kästner, M., Zimmermann, M., 2022b. Structure-property relationships of imperfect additively manufactured lattices based on triply. Materials & Design 222, p. 111036.

Ataee, A., Li, Y., Brandt, M., Wen, C., 2018. Ultrahigh-strength titanium gyroid scaffolds manufactured by selective laser melting (SLM) for bone implant applications. Acta Materialia 158, p. 354.

Raßloff, A., Schulz, P., Kühne, R., Ambati, M., Koch, I., Zeuner, A., Gude, M., Zimmermann, M., Kästner, M., 2021. Accessing pore microstructure–property relationships for additively manufactured materials. GAMM-Mitteilungen 44.